

Quantitative mapping of chlorhexidine in natural river biofilms

James J. Dynes^a, John R. Lawrence^b, Darren R. Korber^c, George D.W. Swerhone^b,
Gary G. Leppard^d, Adam P. Hitchcock^{a,*}

^a Brockhouse Institute for Materials Research, McMaster University, Hamilton, ON, Canada L8S 4M1

^b National Water Research Institute, 11 Innovation Blvd., Saskatoon, SK, Canada S7N 3H5

^c Applied Microbiology and Food Science, University of Saskatchewan, Saskatoon, SK, Canada S7N 5A8

^d National Water Research Institute, PO Box 5050, Burlington, ON, Canada L7R 4A6

Received 28 February 2006; received in revised form 21 April 2006; accepted 27 April 2006

Available online 13 June 2006

Abstract

Soft X-ray scanning transmission X-ray microscopy has been applied to map chlorhexidine, a ubiquitous antimicrobial agent, relative to major biochemical components (proteins, lipids, polysaccharides, Ca^{2+} , K^+ , CO_3^{2-}) in natural river biofilms. For the first time, bio-accumulation of chlorhexidine in diatoms has been observed unambiguously. The quantitative results show that chlorhexidine bioaccumulated extensively in lipid-rich regions of diatoms and bacteria. Confocal laser scanning microscopy was used to document changes in the biofilm community. The bioaccumulation provides a significant entry point for chlorhexidine into the aquatic food chain. It results in modification of the biofilm community and it impacts the photosynthetic and protozoan species in particular. X-ray microscopy mapping at high spatial resolution is shown to be a powerful tool for studies of antimicrobial agents in the environment.

© 2006 Elsevier B.V. All rights reserved.

Keywords: Biofilms; Antimicrobials; Chlorhexidine; X-ray microscopy; STXM; NEXAFS

1. Introduction

Antimicrobial agents, found in personal care products, used in industrial processes, and applied to foodstuffs and medical equipment, enter aquatic ecosystems from industrial and municipal wastewaters (Wilson et al., 2003). Many of these compounds persist after their release into the aquatic ecosystem and retain their “biological activity” (Kolpin et al., 2002; Beek et al., 2000). Subsequently, their interaction with non-

target microorganisms within naturally occurring microbial biofilms could have a significant impact on the microbial ecology of aquatic ecosystems since microbial biofilms represent the lowest trophic level. Understanding the ecological impact of an antimicrobial agent on a natural biofilm requires knowledge of the amount bioaccumulated, its spatial distribution, the biochemistry of the sorption sites, and the impact on biofilm structure, species and viability. Here we show how soft X-ray scanning transmission X-ray microscopy (STXM), when combined with other probes of microbiology and bioavailability, can provide the quantitative mapping needed to answer these questions.

A number of techniques can quantitatively measure the spatial distributions of organic compounds, such as

* Corresponding author. Brockhouse Institute for Materials Research, McMaster University, 1280 Main St. W, Hamilton, ON, Canada L8S 4M1. Tel.: +1 905 525 9140x24749; fax: +1 905 521 2773.

E-mail address: aph@mcmaster.ca (A.P. Hitchcock).

antimicrobial agents and bio-macromolecules (e.g., protein, lipids), in hydrated biological samples. However, mapping by infrared ($\sim 5 \mu\text{m}$) or Raman ($\sim 1 \mu\text{m}$) microscopy is limited by spatial resolution (Suci et al., 2001). Optical techniques have slightly better spatial resolution ($\sim 0.5 \mu\text{m}$) but require fluorescent probes which can introduce artifacts and are limited by the availability of appropriate probes (Hope and Wilson, 2004, 2003; Lawrence et al., 2003). State-of-the-art X-ray fluorescence analysis using hard X-ray synchrotron excitation has a spatial resolution of 150 nm (Kemner et al., 2004); however, only elemental specificity is possible. In principle, organic antimicrobials can be mapped if one attaches a marker atom (or, for chlorhexidine, uses the intrinsic Cl K α fluorescence signal), but this would only provide spatial localization and quantitation, without direct chemical identification. Energy dispersive X-ray spectroscopy (EDX) in a transmission electron microscope (TEM) has a spatial resolution of about 3 nm but it is also limited to elemental specificity, and it has lower sensitivity than synchrotron X-ray absorption or fluorescence.

Soft X-ray scanning transmission X-ray microscopy (STXM) (Ade and Urquhart, 2002; Ade, 1998) provides chemical speciation via near-edge X-ray absorption fine structure (NEXAFS) with a spatial resolution better than 50 nm. With suitable reference spectra, sequences of images recorded over a span of photon energies at core excitation edges can be converted to quantitative maps of specific chemicals in biological samples in hydrated environments. Recently, we have demonstrated the power of STXM to map bio-macromolecules (Lawrence et al., 2003) and metallic species (Fe $^{2+}$, Fe $^{3+}$, Mn $^{2+}$, Ni $^{2+}$) (Dynes et al., 2006) in river biofilms.

Chlorhexidine (1,1'-hexamethylene-bis[5-(*p*-chlorophenyl) biguanide]) is one of the most widely used antimicrobial agents, included in surgical scrubs, health care personnel soaps, preoperative skin preparations, skin antiseptics, skin cleansers, wound protectants, urinary irritants, burn ointments, acne creams, cosmetic preservatives, ophthalmic solution, and oral products such as mouth rinses and toothpaste (Ranganathan, 1996). Here we report a study of the spatial distribution of chlorhexidine following an 8-week exposure of a bacterial–algal river biofilm to river water containing 100 $\mu\text{g L}^{-1}$ (100 ppb) of chlorhexidine digluconate. Confocal laser scanning microscopy (CLSM) with imaging of fluorescence markers was used to characterize specific structures (i.e., microbial species and extracellular polymeric substances (EPS)) in the biofilm. STXM measurements were used to quantitatively map chlorhexidine, protein, lipids, poly-

saccharides, Ca $^{2+}$, K $^{+}$, CO $_3^{2+}$ and silica (SiO $_2$) in two diatom species and a bacterial colony in the biofilm.

2. Methods

2.1. Sample preparation

The methodology has been described in detail elsewhere (Dynes et al., 2006; Lawrence et al., 2002, 2000). In brief, river biofilms were grown on the surface of removable polycarbonate slides in a rotating annular reactor at a water temperature of $17 \pm 2 \text{ }^\circ\text{C}$, a flow rate of 20 mL h^{-1} and a surface velocity of 2 km h^{-1} . Natural river water (South Saskatchewan River, Saskatoon, Saskatchewan, Canada) collected in September and October 2004 was used as inoculum and as the sole source of nutrients. The river water properties were conductivity $450 \mu\text{mhos cm}^{-1}$, pH 8.5, turbidity 2.3 NTU, total Kjeldahl N 24 mg L^{-1} , and total hardness $185 \text{ mg CaCO}_3 \text{ L}^{-1}$. The river water was supplemented with chlorhexidine digluconate to a final concentration of $100 \mu\text{g L}^{-1}$. A control biofilm without exposure to chlorhexidine digluconate, and a nutrient control biofilm, supplemented with the nutrient equivalent (C, N) of chlorhexidine digluconate (C added as sodium gluconate and glucose, and N added as ammonium chloride) but not exposed to chlorhexidine digluconate were also grown under identical conditions. At the end of 8 weeks, the polycarbonate slides were removed from the reactor; all the biofilm ($\sim 40 \mu\text{m}$ thick) was aseptically scraped from the entire slide (11 cm^2) with a silicone spatula and placed in a sterile 1-mL centrifuge tube. No homogenization of the sample was undertaken as the goal was to look at as intact a biofilm as possible. An aliquot of the biofilm material was placed onto an X-ray transparent silicon nitride membrane (Silson Ltd, Northampton, UK) and a second silicon nitride membrane was aligned and placed on top of the wet biofilm; the silicon nitride sandwich (wet cell) was then sealed with acid-free silicone sealant and examined by STXM. The wet cell was stored at $4 \text{ }^\circ\text{C}$ when not being examined by X-ray microscopy.

2.2. Reference compounds

The reference compounds were chlorhexidine digluconate, chlorhexidine dihydrochloride, human serum albumin (protein), xanthan gum (polysaccharide), 1,2-dipalmitoyl-*sn*-glycero-3-phosphocholine (lipid), K $_2$ CO $_3$ and CaCO $_3$. All compounds were from Sigma-Aldrich except human serum albumin (Behringwerke AG) and were of a minimum purity of 98%. In each

case, small amounts were dissolved/dispersed in unbuffered, deionized, distilled water, deposited on silicon nitride membranes and air-dried before STXM analysis.

2.3. Scanning transmission X-ray microscopy and data analysis

X-ray imaging and spectromicroscopy were carried out at the Advanced Light Source (Berkeley, CA) using the STXM microscope at beamline 5.3.2 (Kilcoyne et al., 2003; Warwick et al., 2002). The as-measured transmitted signals were converted to optical densities (OD, absorbance) using incident flux measured through regions of the wet cell devoid of biofilm, to correct for the absorbance by the silicon nitride membranes and the water in the wet cell. After each analytical measurement, an image was recorded at 289 eV, an energy which readily visualizes radiation damage to polysaccharides, the most easily damaged chemical component. The extra-cellular matrix polysaccharide signal was reduced by less than 20% in the worst case of the measurements reported here. The microscope energy scale was calibrated to an accuracy of ± 0.05 eV using sharp gas phase signals, typically the Rydberg peaks of CO_2 .

STXM was used analytically by measuring image sequences at specific energies (Jacobsen et al., 2000) or from image difference maps which are the difference of on- and off-resonance images. For the pennate diatom (diatom 1) the image sequence consisted of 160 images, each of dimension 300×125 pixels, and a dwell time of 1 ms/pixel (total acquisition time was 2.5 h). For the centric diatom (diatom 2) and bacterial colony the image sequence consisted of 173 images, each of dimension 161×88 pixels, and a dwell time of 1 ms/pixel (total acquisition time was 3.5 h). Quantitative maps of chlorhexidine, protein, lipid, polysaccharide, silica (SiO_2), CO_3^{2-} and K^+ were derived from image sequences measured between 280 eV and 320 eV by using singular value decomposition (SVD) (Dynes et al., 2006; Pecher et al., 2003; Jacobsen et al., 2000) to fit the spectrum at each pixel to a linear combination of reference spectra of the components suspected to be present.

The reference spectra, recorded from pure materials, were placed on absolute linear absorbance scales by matching them to the predicted response for the compound based on its elemental composition and density, using tabulated continuum absorption coefficients (Henke et al., 1993). In order to map K^+ independently of the counter anion, the reference spectrum of 'pure K^+ ' was derived by subtracting an appropriately weighted spectrum of CaCO_3 from that of

K_2CO_3 . The X-ray absorption spectrum of silica (SiO_2) is a slowly varying featureless signal in the C 1s region. Thus, its reference spectrum was taken from tabulated elemental absorption coefficients (Henke et al., 1993) and the composition and density of SiO_2 . Although the spectral response for other compounds lacking carbon would also be structure-less in this region, because the frustules are nearly pure ($\sim 97\%$) hydrated silica (SiO_2) (Noll et al., 2002) and are the dominant non-organic component of these systems, the component maps derived from fitting the silica component do represent the spatial distribution of SiO_2 . The Ca^{2+} was mapped from the difference in optical density (OD) images at 352.5 eV ($\text{Ca } 2p_{1/2} \rightarrow \text{Ca } 3d$ resonance) and at 350.3 eV (in the dip between the $2p_{3/2}$ and $2p_{1/2}$ resonances). The ΔOD scale was made quantitative by scaling by $0.10(2) \text{ nm}^{-1}$, the difference in the linear absorbance of nm of CaCO_3 at these two photon energies. The qualitative "biology maps" are the difference of OD images recorded at 288.2 eV (peak of the $\text{C } 1s \rightarrow \pi^*_{\text{C=O}}$ signal of protein) and 282 eV (prior to the onset of C 1s absorption signal). All image and spectral processing was performed with aXis2000 (Hitchcock, 2006).

2.4. Evaluation of STXM data analysis methodology

The reliability of any given component mapping result was evaluated in a number of ways. The derivation of the component maps involved an integrated consideration of a number of different quality checks. One check was the residual image which is constructed from the difference between fit and data at each pixel, averaged over the image sequence energy range. A good quality fit typically has a low magnitude and absence of structure in the residual image. A second check was to examine the fit of the spectrum of 'hot spots' identified by applying a grayscale threshold technique to the component map. This check involved ensuring that the characteristic features of that component were visible, either directly, or after removal of some other dominant component located at the same point. A third check was to explore the optimum number of chemical components in any given image sequence fitting procedure. Principle component analysis of each image sequence indicated that 7 or 8 components could be extracted meaningfully. Spectral fits with 6 (protein, polysaccharide, lipid, chlorhexidine, SiO_2 and CaCO_3), 7 (as for 6, plus K^+), and for 8 (as for 7, plus water) were all explored, for each image sequence. In addition, we explored several alternate model compounds for the protein, polysaccharide, lipid and chlorhexidine components.

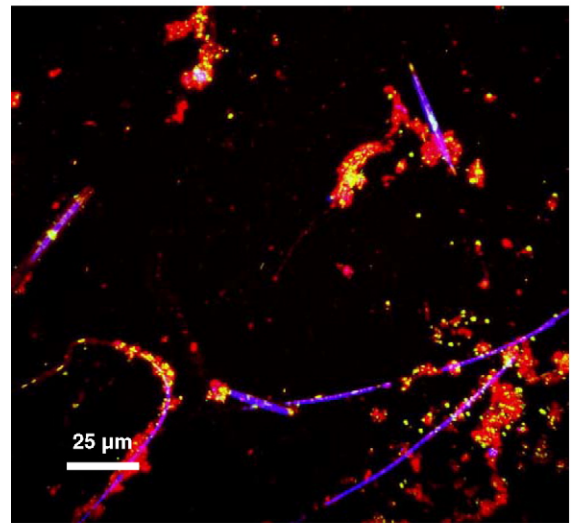
The component maps reported in this paper are typical of this range of analyses. This multi-step evaluation was used to gain confidence that the final result was relatively independent of the exact details of the analysis used. The spatial distributions derived in all the SVD analyses were very similar, but the magnitudes of the thickness scales were considerably more variable (for weaker components, fluctuating by factors of two). An ‘intuitive’ estimate of the reliability (reproducibility) of the quantitation based on this rather extensive, and admittedly somewhat subjective, analysis process is 20% uncertainty in the majority components (maximum contributions greater than 50 nm), and 50% uncertainty in the scales for the minority components (maximum contributions less than 50 nm). These values reflect mostly systematic errors related to our limited knowledge of the actual composition and thus inability to provide an accurate set of reference spectra. The point-to-point precision of any component map is actually very good—a few percent for all but the very weak components—because they are the result of signal contributions from many images.

2.5. Confocal Laser Scanning Microscopy (CLSM) and probes

CLSM image sequences were collected using an MRC 1024 confocal laser scanning microscope (Bio-Rad, Hemel Hempstead, United Kingdom) attached to a Microphot SA microscope (Nikon, Tokyo, Japan) equipped with a 40×, 0.55 numerical aperture (NA) (Nikon), 10×, 0.3 NA (Nikon) and 63×, 0.9 NA lens (Zeiss, Jena, Germany). Biofilms for CLSM analysis were stained with SYTO 9 (Molecular Probes) and the fluor conjugated lectin *Triticum vulgare* (TRITC) (Sigma-Aldrich). SYTO 9 (excitation/emission 488/522 nm) targets the nucleic acids of bacteria and is recorded in the green channel. *T. vulgare* (excitation/emission 568, 605/32 nm) targets the EPS of the biofilm and is recorded in the red channel. The photosynthetic organisms (i.e., algae, cyanobacteria) autofluoresce (excitation/emission 647/680 nm) and are recorded as the blue channel (Neu et al., 2004). The cyanobacteria also autofluoresces (excitation/emission 568, 605/32 nm) and are also recorded in the red channel along with the EPS. Subsequently, to determine the amount of cyanobacteria in the biofilm, the biofilm was not stained with *T. vulgare*. In the 3 channel projections of these image series, the cyanobacteria appear as magenta since they are recorded in both the blue and red channels, the bacteria appear as green (where SYTO 9 staining occurs alone) and yellow (where SYTO 9 and *T. vulgare*-EPS

staining register at the same location) since they are recorded in the green and red channel. Biofilm component volume was determined by image analysis (Lawrence et al., 2002) of the CLSM image sequences. The number of protozoa in the biofilm was determined by visually counting them each week on a 2-cm² piece of the polycarbonate slide while looking through a microscope. The protozoans were mainly ciliates and flagellates. The cumulative number of protozoa from the final four weeks is reported.

(a) control



(b) chlorhexidine

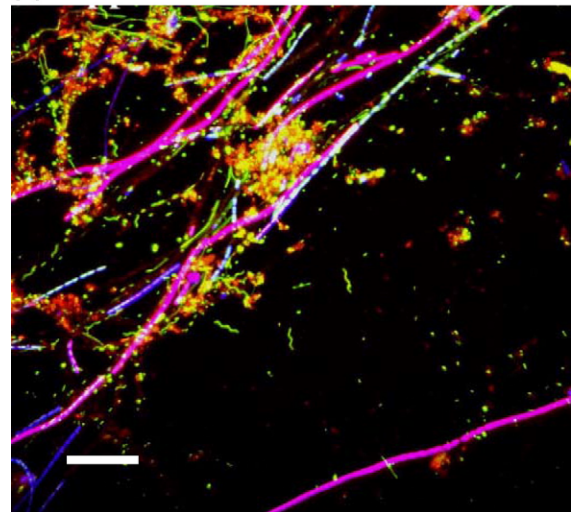


Fig. 1. Confocal laser scanning microscopy (CLSM) images of (a) control and (b) chlorhexidine biofilms, illustrating the distributions of algae (blue), cyanobacteria (magenta), bacteria (green, yellow) and EPS (red). The biofilm was stained with *T. vulgare* (red) and SYTO 9 (green). Autofluorescence of algae is recorded as blue; cyanobacteria are recorded as blue and red.

3. Results

The CLSM images of the control and chlorhexidine biofilms (Fig. 1) showed that they were both very rich bacterial–algal communities with a variety of complex architectures and microbial compositions. The analysis of the CLSM images indicated that the total amount of the biofilm components (i.e., algae, cyanobacteria and bacteria) was lower for the control biofilm ($0.5 \mu\text{m}^3 \mu\text{m}^{-2}$) compared to that of the chlorhexidine treated biofilm ($2.5 \mu\text{m}^3 \mu\text{m}^{-2}$) and the nutrient control biofilm ($1.7 \mu\text{m}^3 \mu\text{m}^{-2}$). However, the community composition of the biofilm was altered in the presence of chlorhexidine, as evident from the percentage of algae/cyanobacteria/bacteria in the chlorhexidine (35/5/60%) versus the control (75/5/20%) and nutrient control (40/20/40%) biofilms. The number of grazers (protozoans) observed in the control biofilm (10 protozoan/cm²) was considerably higher than that of the chlorhexidine biofilm (1 protozoan/cm²) but less than the nutrient control (28 protozoan/cm²). The nutrient control results showed that the effect of the chlorhexidine on the biofilm was not due to the increased nutrient levels from the chlorhexidine digluconate itself but from its antimicrobial effects.

Fig. 2 shows STXM images at 288.2 eV of the pennate (diatom 1) and centric (diatom 2) diatoms and of the bacterial colony examined in detail in this study. At this photon energy microbial organisms are preferentially visualized, mainly due to absorption by the strong $C\ 1s \rightarrow \pi^*_{C=O}$ peptide band of proteins. Fig. 2b is an image difference map ($I_{288.2} - I_{282}$) of the region of diatom 1 subjected to detailed study. This image difference is useful in that it shows only the organic components of the biology and removes the strong contribution from other components, such as the silica frustule. Fig. 2c is the STXM image at 288.2 eV of the centric diatom (diatom 2) and of the adjacent bacterial colony. The pennate diatom was part of a colony whereas the centric diatom was solitary; both were

found in association with dense and morphologically diverse bacterial colonies. Fig. 2d is the image difference ($I_{288.2} - I_{282}$) of a pennate diatom colony

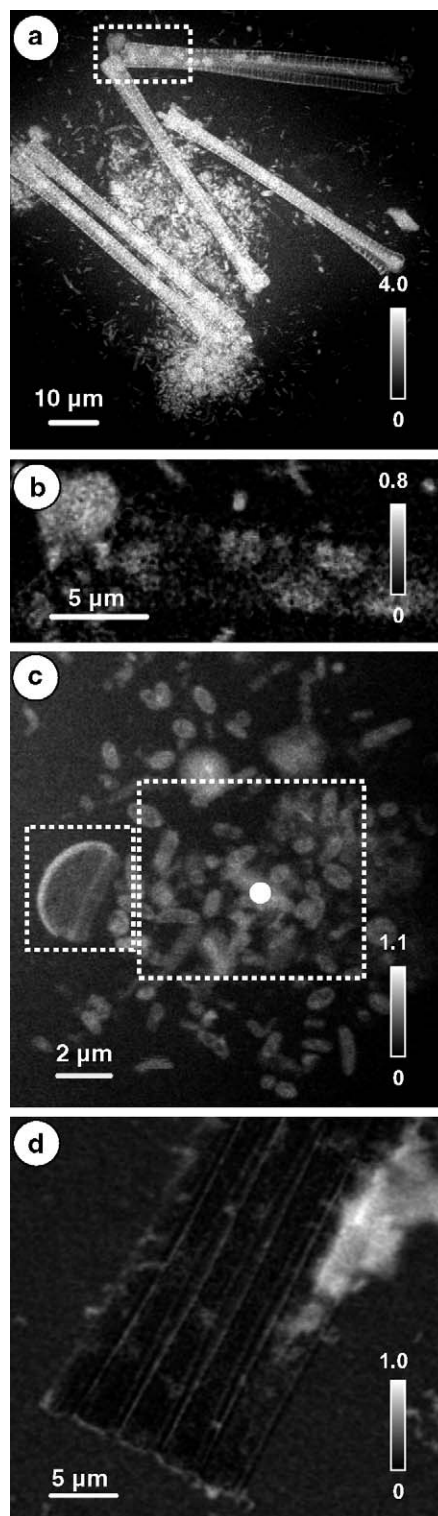


Fig. 2. Optical density (OD) images of a river biofilm exposed for 8 weeks to $100 \mu\text{g L}^{-1}$ chlorhexidine, recorded by scanning transmission X-ray microscopy (STXM). (a) Region of the pennate diatom colony (diatom 1). (b) Difference in OD images at 288.2 and 282 eV of the area in the white rectangle in (a). This difference image highlights the organic components of the biofilm. (c) The 288.2 eV image of the region of the centric diatom (diatom 2) and bacterial colony in the chlorhexidine-exposed biofilm. The white rectangles show the areas of detailed study. (d) OD image difference (288.2–282 eV) of a pennate diatom colony from the control biofilm (no chlorhexidine exposure). The gray scales indicate optical density or optical density difference.

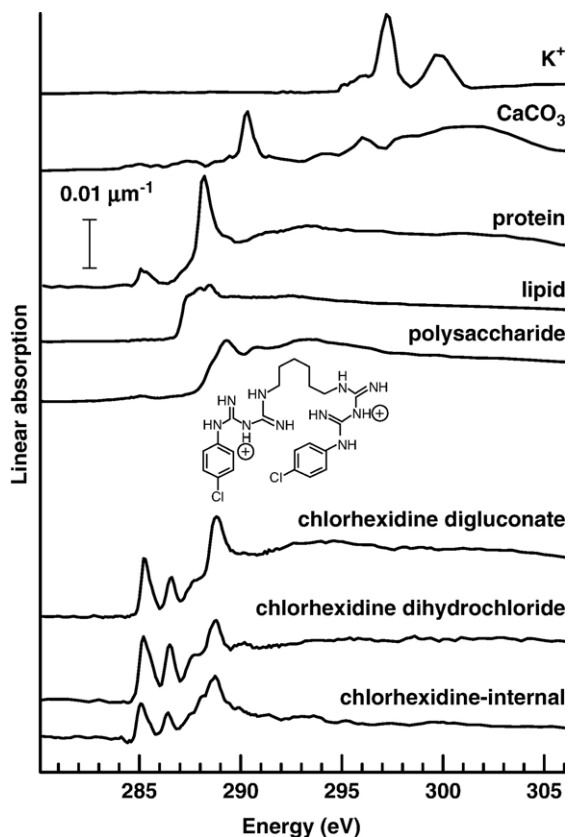


Fig. 3. X-ray absorption reference spectra. The spectra of pure K^+ (K_2CO_3 with CO_3^{2-} subtracted), $CaCO_3$, protein (human serum albumin), lipid (1,2-dipalmitoyl-*sn*-glycero-3-phosphocholine), polysaccharide (xanthan gum), chlorhexidine digluconate, chlorhexidine dihydrochloride are plotted on an absolute linear absorbance scale with offsets. The spectrum extracted from a 500-nm-diameter region at the white dot in Fig. 2c (chlorhexidine-internal) shows excellent agreement with the spectrum of pure chlorhexidine in the region of the characteristic $C\ 1s \rightarrow \pi^*$ transitions (284–289 eV).

from the control biofilm that was not exposed to chlorhexidine, but otherwise identically treated.

The spectra of the six reference compounds (protein, lipid, polysaccharide, K_2CO_3 , $CaCO_3$ and chlorhexidine dihydrochloride) are presented in Fig. 3. The shapes of the $C\ 1s$ spectra of protein, polysaccharide and lipids are characteristic of these species (Lawrence et al., 2003). The $C\ 1s$ spectrum of $CaCO_3$ (Lawrence et al., 2003) and the $K\ 2p$ spectrum of K_2CO_3 (Sette et al., 1989)

have been reported previously. This is the first report of the $C\ 1s$ spectra of chlorhexidine digluconate and chlorhexidine dihydrochloride to our knowledge. While

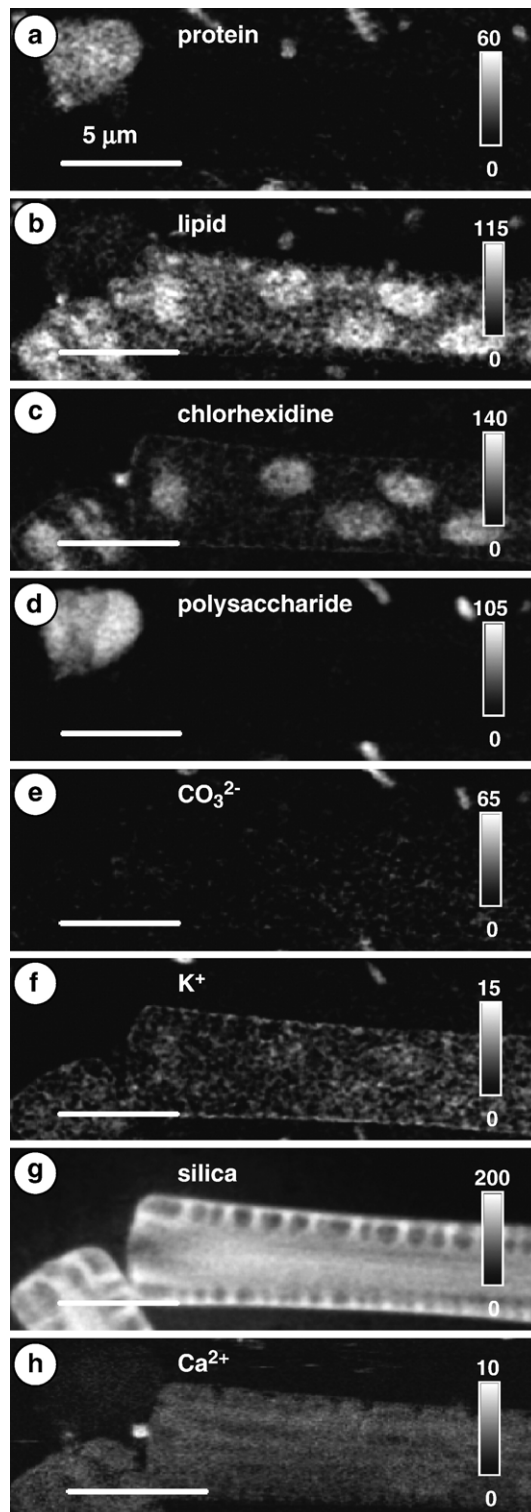


Fig. 4. Diatom 1 component maps. (a) Protein, (b) lipid, (c) chlorhexidine, (d) polysaccharide, (e) CO_3^{2-} , (f) K^+ , (g) silica and (h) Ca^{2+} . Maps (a–g) were derived by singular value decomposition (SVD) of an image sequence (280–320 eV). The Ca^{2+} map (h) was derived from an image difference (352.6–350.3 eV). The gray scales indicate thickness in nanometers.

not identical, due to different contributions from the counter-anions, the spectra of these two chlorhexidine species both exhibit characteristic sharp features at 285.1 and 286.4 eV, associated with $C\ 1s \rightarrow \pi^*_{\text{ring}}$ and $C\ 1s \rightarrow \pi^*_{C=N}$ transitions in the phenyl and imide groups of this molecule. Based on these features, chlorhexidine is readily differentiated from biological molecules. It is very likely that the cation and anion of the as-introduced chlorhexidine digluconate would be incorporated separately into the biofilm. Thus, we chose to use the spectrum of chlorhexidine dihydrochloride as the reference for all analyses since this $C\ 1s$ signal is exclusively from the chlorhexidine cation. It is also likely that the gluconate is metabolized by the microbial organisms. In fact, regardless of which chlorhexidine

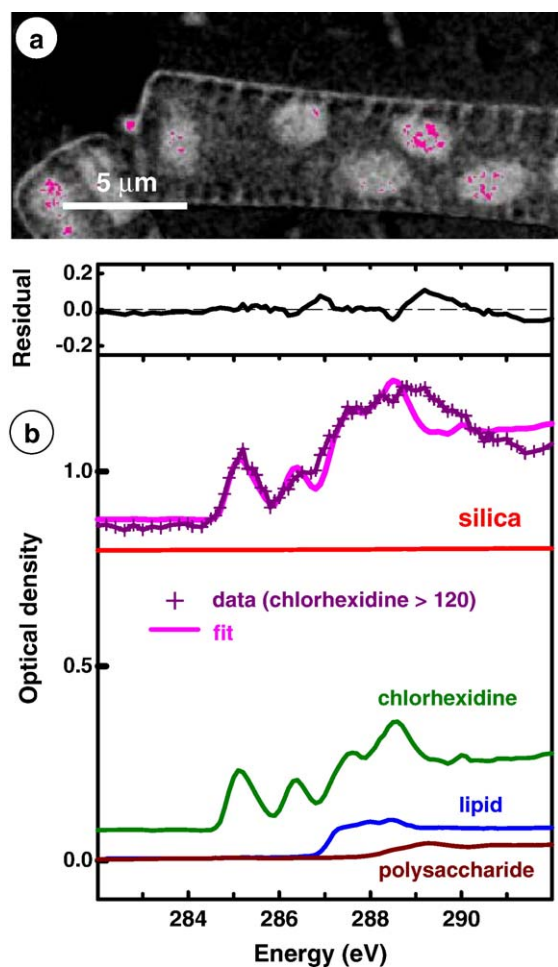


Fig. 5. (a) Chlorhexidine component map, with pixels having values >120 nm superimposed in pink. (b) Curve fit to the spectrum extracted from these pixels. The levels of protein and Ca^{2+} were very low and are not plotted; K^+ and CO_3^{2-} , also low, were not included in this fit. See Table 1 for numerical details of this fit, as well as for fits to spectra extracted with lower thresholds (>80 and >100 nm).

Table 1

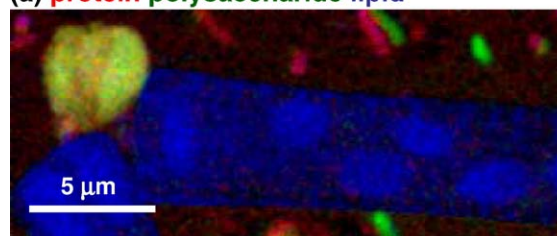
Results from curve fit of extracted signals with large chlorhexidine content identified by threshold masking the chlorhexidine component map for diatom 1

Component	Thickness (nm)		
	>80	>100	>120
Protein (albumin)	-0.5	-1.0	-1.6
Polysaccharide (xanthan gum)	0.7	0.5	0.9
Lipid (1,2-dipalmitoyl- <i>sn</i> -glycero-3-phosphocholine)	7.2	7.0	5.5
Chlorhexidine (as dihydrochloride)	42	58	79
Silica	146	142	131
CO_3^{2-}	NI	NI	NI
K^+	NI	NI	NI
Standard deviation of fit	0.028	0.031	0.033

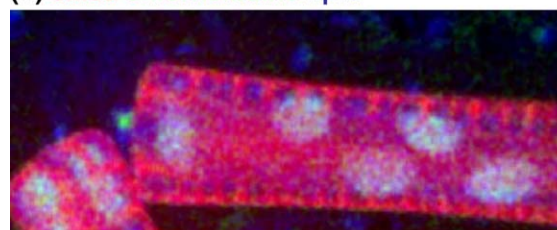
NI—not included in the fit.

species was used in the fitting, the spatial distribution and quantitation of the components were similar, indicating that any systematic errors associated with the selection of the reference chlorhexidine spectrum are

(a) protein polysaccharide lipid



(b) silica chlorhexidine lipid



(c) Ca^{2+} chlorhexidine K^+

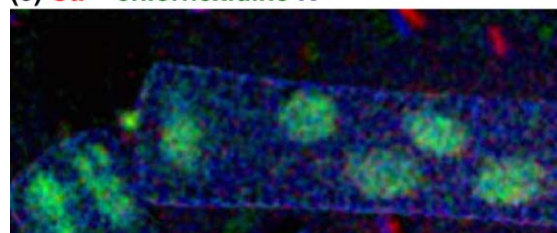


Fig. 6. Color coded composites of selected component maps from diatom 1. (a) Red=protein, green=polysaccharide, blue=lipid. (b) Red=silica, green=chlorhexidine, blue=lipid. (c) Red= Ca^{2+} , green=chlorhexidine, blue= K^+ . The component maps are those from Fig. 4, individually rescaled.

small. The STXM mapping of the major components was performed using the reference spectra shown in Fig. 3 and the derived spectrum of silica.

3.1. Pennate diatom (diatom 1)

Fig. 4 presents quantitative component maps for proteins, lipids, polysaccharides, chlorhexidine, CO_3^{2-} , K^+ , Ca^{2+} and silica of the pennate diatom. The gray scales give the thickness of each component in nanometers. The lipids in the pennate diatom occur mainly as intracellular spherical inclusions (droplets) and as a small lipid droplet external but adjacent to the frustule. Chlorhexidine was unambiguously detected in

the diatom. An example of the spectral basis for identification of the chlorhexidine is given in Fig. 3, which shows very close correspondence of the C 1s spectrum extracted from a 500-nm-diameter region of the bacterial colony of the biofilm (location defined by white circle in Fig. 2c) and the C 1s spectrum of the two reference chlorhexidine compounds. In less concentrated areas, the chlorhexidine signal overlaps that of the bio-macromolecules and requires spectral fitting to identify. An example of the spectral fitting is shown in Fig. 5. The spectrum of a chlorhexidine-rich region was extracted from the image sequence using threshold masking of the chlorhexidine component map to include only pixels with a value of 120 nm or larger, which are

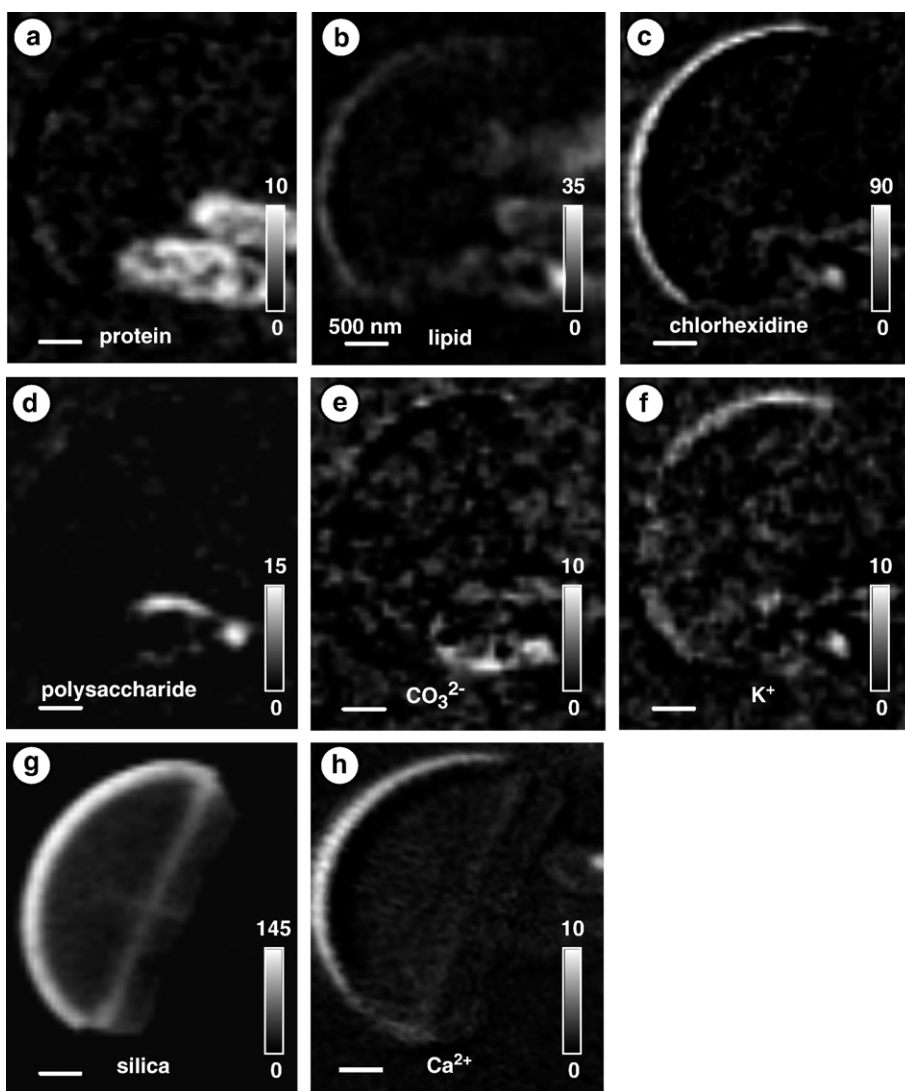


Fig. 7. Component maps for diatom 2. (a) Protein, (b) lipid, (c) chlorhexidine, (d) polysaccharide, (e) CO_3^{2-} , (f) K^+ , (g) silica and (h) Ca^{2+} . See caption to Fig. 4 for further details.

identified in Fig. 5a. The spectral shape and fit show that chlorhexidine is detected in the lipid droplet regions. Fig. 5b is the energy domain fit to the spectrum of those pixels. The residuals are small and unstructured indicating that, while the fit is not perfect, it is reasonable, and there is clearly signal at the energies of the two sharp low lying C $1s \rightarrow \pi^*$ transitions characteristic of chlorhexidine. The numerical details of this fit, as well as fits to signals from two other sets of pixels in the lipid–chlorhexidine droplets, are presented in Table 1.

Fig. 6 shows color composites of selected component maps indicating the spatial correlation of the components. Clearly, chlorhexidine was bioaccumulated in the intracellular and the extracellular lipid droplets of the diatom. Among the components mapped, the chlorhexidine constituted $\sim 25\%$ and $\sim 40\%$ of the intracellular and extracellular droplets, respectively. The lipid constituted $\sim 25\%$ of the droplets. Considering that the biofilm was only exposed to $100 \mu\text{g L}^{-1}$ of chlorhexidine, this level of bioaccumulation in an 8-week period is remarkable.

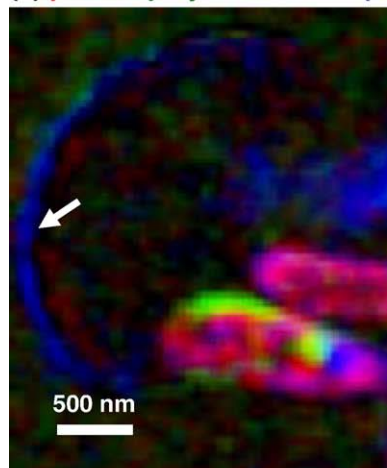
Previous research (Noll et al., 2002) has shown that diatom frustules are composed of almost pure hydrated silica (SiO_2) ($\sim 97\%$), with the remainder being organic components ($\sim 3\%$) and trace amounts of other elements. The STXM mapping shows that the frustule was composed mainly of SiO_2 , with small amounts of K^+ and Ca^{2+} . A distinct pattern (meshed or network) was observed in the spatial distribution of the K^+ associated with the frustule. In contrast, Ca^{2+} was uniformly distributed over the frustule although there was also a strong concentration of Ca^{2+} in association with the external chlorhexidine–lipid droplet. The different spatial distributions of K^+ and Ca^{2+} are perhaps due to specific morphological or biogenic characteristics of the frustule of this particular pennate diatom (Noll et al., 2002; Crawford et al., 2001).

3.2. Centric diatom (Diatom 2)

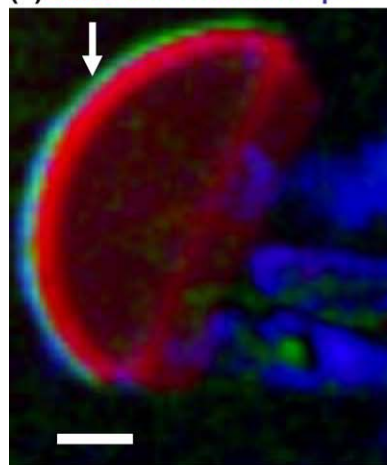
Fig. 7 presents the quantitative component maps for protein, lipids, polysaccharides, chlorhexidine, CO_3^{2-} , K^+ , Ca^{2+} and silica of a centric diatom. The spatial

correlations for selected component maps are shown in Fig. 8. As in diatom 1, chlorhexidine was detected in clear association with lipids. However, in contrast to the

(a) protein polysaccharide lipid



(b) silica chlorhexidine lipid



(c) Ca^{2+} chlorhexidine K^+

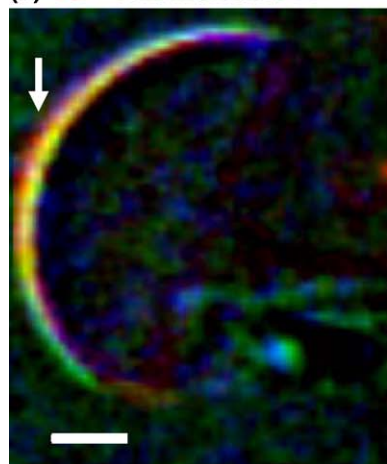


Fig. 8. Color coded composites of selected component maps from diatom 2. (a) Red=protein, green=polysaccharide, blue=lipid. (b) Red=silica, green=chlorhexidine, blue=lipid. (c) Red= Ca^{2+} , green=chlorhexidine, blue= K^+ . The component maps are those from Fig. 7, individually rescaled. The arrows indicate the lipid, chlorhexidine and Ca^{2+} association along the outside of the diatom frustule.

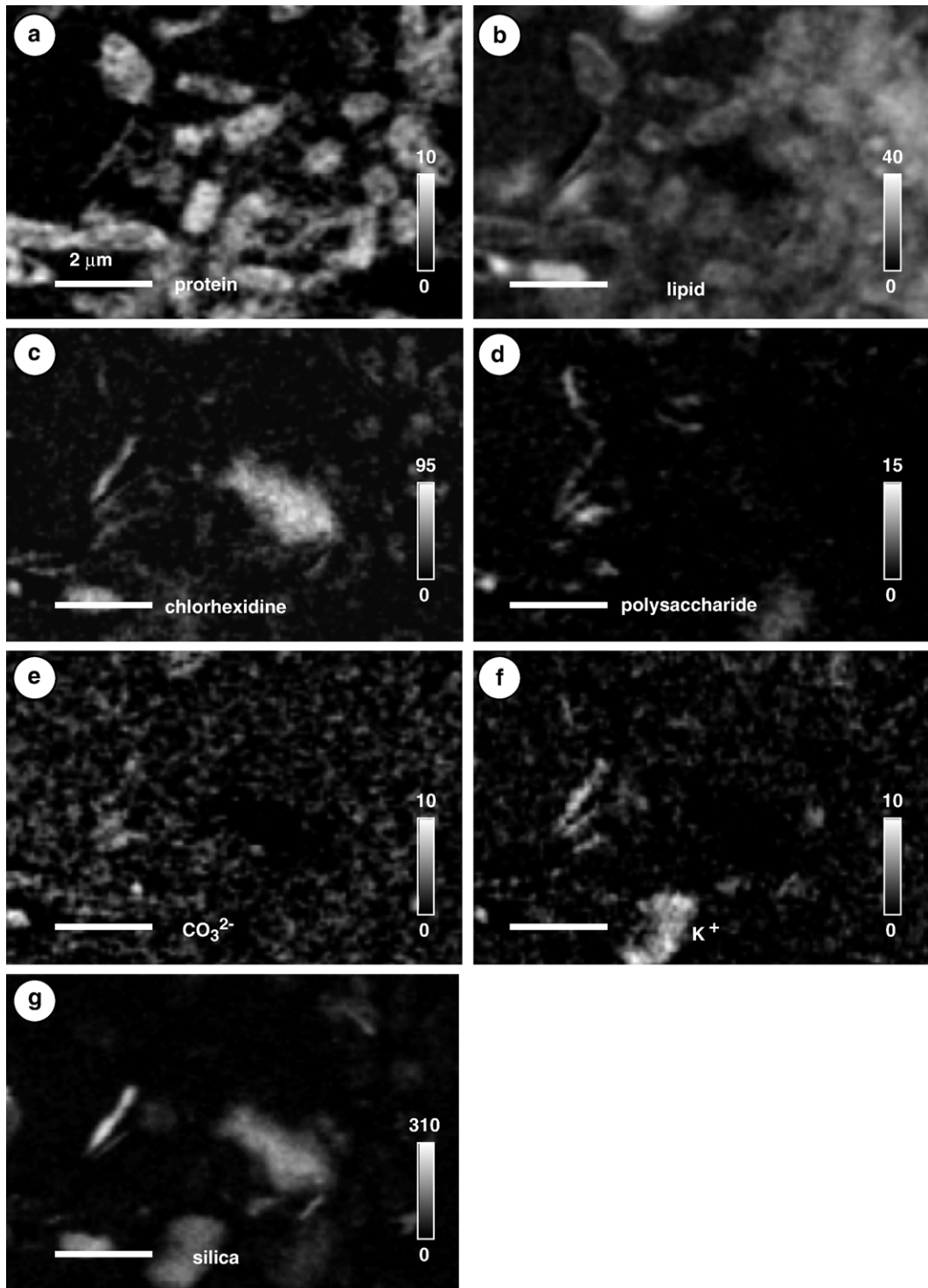


Fig. 9. Component maps for the bacterial colony. (a) Protein, (b) lipid, (c) chlorhexidine, (d) polysaccharide, (e) CO_3^{2-} , (f) K^+ and (g) silica. See the caption to Fig. 4 for further details.

pennate diatom, the chlorhexidine in the centric diatom only occurred in a lipid layer external to the frustule, rather than in association with intracellular or extracellular lipid droplets. Chlorhexidine was $\sim 50\%$, whereas the lipids were $\sim 25\%$ of the components mapped in the lipid layer external to the frustule. As in diatom 1, a very substantial bioaccumulation of chlorhexidine was observed. In agreement with the pennate diatom case, the chlorhexidine-rich lipid layer also contained Ca^{2+} and K^+ .

The chlorhexidine–lipid layer was at most 80 nm wide—there may be some contributions to the apparent width from the spatial resolution (~ 40 nm) and possible image-to-image misalignment. In contrast, the dense siliceous part of the frustule adjacent to the chlorhexidine–lipid layer was about 240 nm wide.

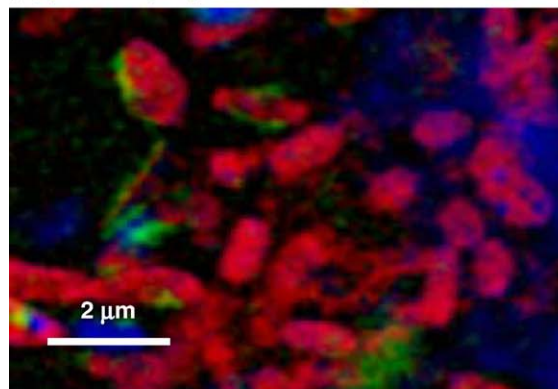
3.3. Bacterial colony

Fig. 9 presents the quantitative component maps for protein, lipids, polysaccharides, chlorhexidine, CO_3^{2-} , K^+ , and silica for a bacterial colony. The spatial correlations for selected component maps are shown in Fig. 10. Chlorhexidine was observed to be associated with the lipids in the bacteria. Among the components mapped, the chlorhexidine and lipids constituted $\sim 10\%$ and $\sim 30\%$, respectively of the intracellular material. Chlorhexidine also appeared to be associated with some materials which were highlighted in the silica component map. These could be remnants of diatom frustules; however, since it was not possible to visually confirm that, we cannot rule out the possibility that the chlorhexidine is associated with some non-carbonaceous material other than silica.

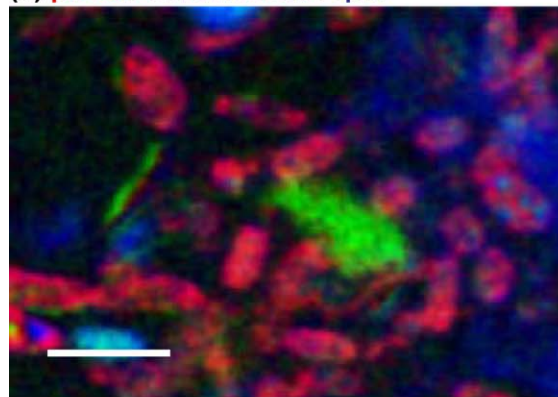
3.4. Control biofilm

Seven species of pennate diatoms from the control biofilm, grown under the same conditions except without the $100 \mu\text{g L}^{-1}$ of chlorhexidine, were examined by STXM and found not to contain lipid droplets. This is illustrated by comparison of the image difference map ($I_{288.2} - I_{282}$) of a colony of four pennate diatoms in the control biofilm (Fig. 2d) to the image (Fig. 2a) or image difference (Fig. 2b) of the pennate diatom from the chlorhexidine exposed biofilm. Similar results (not shown) were obtained for the other six pennate diatom species. Chlorhexidine was not detected in the pennate diatoms or other components of the control biofilm. In particular, chlorhexidine was not detected by STXM in bacterial colonies present in control biofilms. The bacteria were found to contain

(a) protein polysaccharide lipid



(b) protein chlorhexidine lipid



(c) silica chlorhexidine lipid

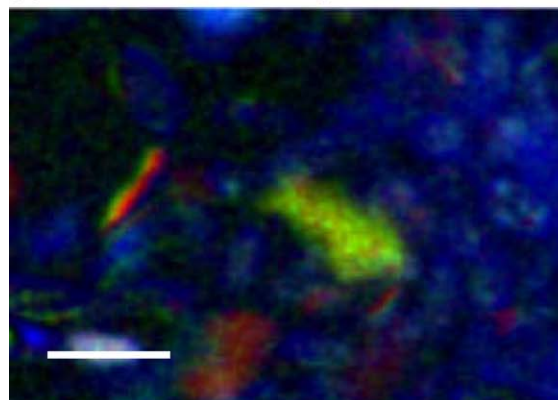


Fig. 10. Color coded composites of selected component maps from the bacterial colony. (a) Red=protein, green=polysaccharide, blue=lipid. (b) Red=protein, green=chlorhexidine, blue=lipid. (c) Red=silica, green=chlorhexidine, blue=lipid. The component maps are those from Fig. 9, individually rescaled.

protein, lipids, and polysaccharides in similar amounts to that observed in the bacteria from the chlorhexidine biofilm (data not shown).

4. Discussion

Numerous studies using traditional methods such as fractionation and extraction techniques, radioactivity and monitoring of biological activity have demonstrated that exposure of pure cultures of bacteria, fungi, yeast and protozoa to chlorhexidine results in its bioaccumulation, which has an impact on the biofilm and cells, including viability, structure and/or biochemistry. For example, Walters et al. (1983) determined the viability of yeast cells by measuring the optical density of the cell suspension, chlorhexidine uptake by measuring adsorption isotherms using whole cells and isolated cell walls, cell membrane integrity by monitoring the release of intracellular materials such as pentose, and a change in cell wall characteristics by determining the charge on the cell surface. These traditional methods were unable to spatially locate the chlorhexidine in situ. CLSM has revealed the structure and spatial distribution of viable cells within a multi-species oral bacterial biofilm (Hope and Wilson, 2004, 2003), but was unable to locate chlorhexidine in the biofilm or shed light on the biochemistry of the chlorhexidine sorption sites. This is consistent with our CLSM results, which indicated the effect of chlorhexidine on the biofilm structure and species composition but provided no information on the amounts of chlorhexidine bioaccumulated or its location relative to the biofilm structures and biochemistry.

Suci et al. (2001) used infrared and Raman spectroscopy to quantify the amount of chlorhexidine sorbed by *Candida albicans* biofilms over time, observing that sorption was higher in the interfacial region versus the bulk biofilm. It was not possible to distinguish between intra- and extra-cellular sorption and a discussion of the correlation of biochemistry to chlorhexidine bioaccumulation was not provided. Spot EDX analyses for chlorhexidine in individual yeast cells (Hiom et al., 1995) detected a chlorine signal but it could not be attributed unambiguously to chlorhexidine, nor was it possible to quantify the amount or determine its spatial localization. Khunkitti et al. (1999) used TEM EDX to show that the chlorine content of protozoa increased in the presence of chlorhexidine. However, the correlation with the introduced chlorhexidine was ambiguous due to the presence of large amounts of chlorine from natural sources. The EDX analysis was not able to supply biochemical information on the chlorhexidine sorption sites.

In the present study, soft X-ray STXM was able to use the intrinsic spectral properties of chlorhexidine to quantitatively map in situ the spatial distribution of chlorhexidine in two diatom species and a bacterial colony. To our knowledge, this is the first time that diatom species have been observed to bioaccumulate chlorhexidine. The chemically specific imaging capabilities of STXM showed explicitly that the chlorhexidine bioaccumulation occurs in both the intra- and extra-cellular components of the diatoms and in the intracellular components of the bacteria.

Chlorhexidine is a positively charged hydrophobic and lipophilic molecule (Castillo et al., 2004; Akaho and Fukumori, 2001). Compounds of this type usually accumulate in the fatty tissues (e.g., lipids) of living organisms. Studies have shown that chlorhexidine (Castillo et al., 2004) and similar compounds (poly (hexamethylene biguanide hydrochloride)) (Ikeda et al., 1983) interact with lipids. Moreover, the ionic interactions of chlorhexidine occur mainly with anionic carboxylate groups of mono-molecular films and not with hydroxyl and amide groups (Fisher and Quintana, 1975). Elferink and Boon (1974) suggested that the loss of K^+ impermeability of yeast cells in the presence of chlorhexidine indicated disruption of the lipid structures of liposomes, suggesting that chlorhexidine interacts with membrane lipids. Microbial resistance to chlorhexidine was attributed to lipopolysaccharides in the outer membrane but not to cell lipid content (Thomas and Stickler, 1979). Broxton et al. (1984) studied the interaction of polyhexamethylene biguanides on the membrane phospholipids in *Escherichia coli*, and indicated that there was a specific interaction between the biguanides and acidic phospholipids. Although there have been no studies on the interaction of chlorhexidine with diatoms, higher sorption of chlorobenzenes, which have similar hydrophobic and lipophilic properties as chlorhexidine, to algae has been related to lipid volume or composition (neutral/polar lipid ratios) (Sicko-Goad et al., 1989a,b). With STXM, it was possible to show unambiguously that chlorhexidine was sorbed or otherwise chemically associated with the lipids in the diatoms and bacteria.

Previous studies (Wernert et al., 2004; Sicko-Goad et al., 1989a,b) have shown extensive association of organo-chlorine compounds with lipids in diatoms. For example, exposure of *Cyclotella meneghiniana*, a centric diatom, to sub-lethal doses of organochlorine compounds such as trichlorobenzene resulted in a significant increase in lipid production, coinciding with the appearance of lipid droplets in the exposed

diatoms but not in the control diatoms (Sicko-Goad et al., 1989a,b). Our results are consistent with these observations. Thus, it appears likely that the formation of lipid droplets in the pennate and centric diatoms was induced by the continuous exposure of the diatoms to $100 \mu\text{g L}^{-1}$ of chlorhexidine over the 8-week period. Sicko-Goad et al. (1989b) hypothesized that the increased lipid stores may alter the timing of response to lipophilic toxicants. Hence, it seems likely that the diatom initiated increased lipid production in response to the presence of chlorhexidine; that is, the strong correlation of lipid and chlorhexidine is not just a consequence of a high affinity of chlorhexidine for lipids (Castillo et al., 2004). The facts that the lipid droplets were not seen in the control diatoms; that chlorhexidine accumulated in an extensive lipid layer external to the frustule in the centric diatom (diatom 2); and that the chlorhexidine was sorbed/chemically associated with the lipids in the pennate diatom (diatom 1), all support models in which lipids are produced by diatoms to absorb and thus isolate the toxic chlorhexidine.

From this study it appears that the diatom species have higher affinity for chlorhexidine than the bacteria examined. Researchers have found there is considerable variation in the response of different types of microorganisms to antimicrobial agents; this has been attributed to differences in cellular physiology and structure (Russell, 2003). The cell membranes of both bacteria and diatoms are composed of phospholipids and lipopolysaccharides, with the hydrophobic groups directed inward and the hydrophilic groups toward the outside, where they associate with water (Brock et al., 1984). Embedded in the cell membrane are hydrophobic proteins. There will be differences in the types of lipids and proteins found in the diatoms and the bacteria. In addition to the cell membrane, the diatom also has a cell wall (i.e., frustule) protecting the cell membrane. The frustule is composed mainly of hydrated silica, with organic compounds (i.e., polysaccharides, proteins) and trace elements embedded in silica (Noll et al., 2002; Crawford et al., 2001). The frustule exhibits a porous network coated with extracellular organic layers. The initial interaction of chlorhexidine with organic molecules is generally thought to occur via electrostatic attraction, whereby the positively charged biguanide groups chemically sorb with negatively charged hydrophilic groups of organic molecules, followed by association of the chlorphenyl and hexane groups (hydrophobic groups of chlorhexidine) with the hydrophobic groups of the organic molecules (Castillo et al., 2004; Akaho and Fukumori, 2001). Presumably, the

chlorhexidine interacts with the phospholipids and lipopolysaccharides on the cell membrane of the bacteria as described above, and then enters the cell through some type of active or passive transport mechanism. For the diatoms species, it is likely that chlorhexidine interacts similarly with the phospholipids and lipopolysaccharides of the cell membrane. However, in some manner the diatom appears to be able to concentrate the chlorhexidine into lipid droplets, presumably as a means to remove and/or prevent its sorption by the cytoplasm and cell membrane. Moreover, the organic compounds associated with the cell wall may play a role in concentrating the chlorhexidine in the lipid droplets. Further study is required to understand why the diatoms bioaccumulate more chlorhexidine (>25%) than the bacteria (<10%). Nevertheless, the differences in the bioaccumulation of chlorhexidine by diatoms and bacteria do indicate that not all species in a natural biofilm will contribute to bioaccumulation to the same degree. Consequently, the degree of antimicrobial bioaccumulation in a biofilm will depend on the presence and abundance of specific species.

There was a greater diversity of algae in the control biofilm than in the chlorhexidine exposed biofilm. This suggests that only algae capable of expressing this protective mechanism persisted in biofilms exposed to chlorhexidine. In contrast, bioaccumulation of chlorhexidine in the lipids of the bacteria was not likely a protective mechanism. We note that chlorhexidine degradation in activated sludge has been reported in the literature (Tanaka et al., 2005). While this may also be a factor in the natural biofilm community, we have not specifically sought evidence for it, but rather have focused on studying bioaccumulation of the unmodified compound.

Lipids in bacteria, algae and microinvertebrates are a significant energy source for higher organisms. The observed bioaccumulation of chlorhexidine by diatoms and bacteria could have significant implications for organisms that feed on them. Possible effects could include biomagnification, prey-avoidance by organisms ingesting lipid-rich cells containing chlorhexidine, reduced grazing, and lower numbers of species that feed on diatoms and bacteria. Other researchers have noted that uptake of organic contaminants by organisms at higher trophic levels occur primarily via their food supply and not by dermal absorption (Wolfaardt et al., 1994; Gossett et al., 1983). The CLSM results from this study showed that the amount of biomass in the chlorhexidine biofilm was higher than the control biofilm, suggesting there was less grazing in the

chlorhexidine biofilm, in keeping with the observed suppression of grazers. These results, and the fact that the chlorhexidine was concentrated in the lipids, are consistent with the reduction in grazers being attributed to ingestion of the bioaccumulated chlorhexidine, rather than absorption. Interestingly, the bioaccumulation of diclofop in natural biofilms occurred in the microbial exopolymers, and also impacted grazers (Wolfaardt et al., 1994).

Diatoms fix a major portion of the Earth's carbon, generate oxygen, cycle nutrients, and are a high-quality food source for a large variety of organisms (Dixit et al., 1992). Bioaccumulation of chlorhexidine by non-target microorganisms such as diatoms, and with subsequent bioconcentration at higher trophic levels, has implications as to the efficacy of antimicrobial action, and the fate of chlorhexidine in natural environments. Hence, the ongoing release into aquatic ecosystems of chlorhexidine and other antimicrobial agents may have a significant impact on the environment and ecosystem health.

In summary, STXM was used to quantitatively map the chlorhexidine and bio-macromolecule spatial distributions in two diatom species and a bacterial colony in a natural river biofilm. Quantitative, high resolution STXM mapping of antimicrobial agents relative to the microbiology and biochemistry of biofilms is furthering our understanding of the impact on aquatic ecosystems of the currently ubiquitous use of broad spectrum antimicrobials, particularly in personal care products. To our knowledge, this is the first high spatial resolution study of chlorhexidine bioaccumulation relative to biochemical composition and structure of a natural, mixed species biofilm.

Acknowledgements

This work was supported by Environment Canada, the Advanced Foods and Materials Network, NSERC (Canada), and the Canada Research Chair program (APH). Construction and operation of the STXM5.3.2 microscope is supported by NSF DMR-9975694, DOE DE-FG02-98ER45737, Dow Chemical, NSERC and the Canada Foundation for Innovation. We thank David Kilcoyne and Tolek Tyliczszak for their contributions to developing and maintaining the instrument. The Advanced Light Source is supported by the Director, Office of Energy Research, Office of Basic Energy Sciences, Materials Sciences Division of the U.S. Department of Energy, under Contract No. DE-AC03-76SF00098.

References

- Ade H. X-ray spectromicroscopy. In: Samson JAR, Ederer DL, editors. *Experimental methods in the physical sciences*, vol. 32. NY: Academic Press; 1998. p. 225–61.
- Ade H, Urquhart SG. NEXAFS spectroscopy and microscopy of natural and synthetic polymers. In: Sham TK, editor. *Chemical applications of synchrotron radiation*. Singapore: World Scientific Publishing; 2002. p. 285–355.
- Akaho E, Fukumori Y. Studies of adsorption characteristics and mechanism of adsorption of chlorhexidine mainly by carbon black. *J Pharm Sci* 2001;90:1288–97.
- Beek B, Bohling S, Bruckmann U, Franke C, Johncke U, Studinger G. The assessment of bioaccumulation. In: Beek B, editor. *The handbook of environmental chemistry*, vol. II (Part J); 2000. p. 239.
- Brock TD, Smith DW, Madigan MT. *Biology of microorganisms*. 4th ed. Englewood Cliffs, NJ: Prentice-Hall, Inc.; 1984. p. 847.
- Broxton P, Woodcock PM, Heatley F, Gilbert P. Interaction of some polyhexamethylene biguanides and membrane phospholipids in *Escherichia coli*. *J Appl Bacteriol* 1984;57:115–24.
- Castillo JA, Pinazo A, Carilla J, Infante MR, Alsina MA, Haro I, et al. Interaction of antimicrobial arginine-based cationic surfactants with liposomes and lipid monolayers. *Langmuir* 2004;20:3379–87.
- Crawford SA, Higgins MJ, Mulvaney P, Wetherbee R. Nanostructure of the diatom frustule as revealed by atomic force and scanning electron microscopy. *J Physiol* 2001;37:543–54.
- Dixit SS, Smol JP, Kingston JC, Charles DF. Diatoms: powerful indicators of environmental change. *Environ Sci Technol* 1992; 26:23–33.
- Dynes JJ, Tyliczszak T, Araki T, Lawrence JR, Swerhone GDW, Leppard GG, et al. Speciation and quantitative mapping of metal species in microbial biofilms using scanning transmission X-ray microscopy. *Environ Sci Technol* 2006;40:1556–65.
- Elferink JGR, Boon HL. Interaction of chlorhexidine with yeast cells. *Biochem. Pharm.* 1974;23:1413–9.
- Fisher RG, Quintana RP. Surface-chemical studies on chlorhexidine and related compounds: II. Interactions with monomolecular-film systems. *J Dent Res* 1975;54:25–31.
- Gossett RW, Brown DA, Young DR. Predicting the bioaccumulation of organic compounds in marine organisms using octanol/water partition coefficients. *Mar Pollut Bull* 1983;14:387–92.
- Henke BL, Gullikson EM, Davis JC. *At Data Nucl Data Tables* 1993;54:181–297.
- Hiom SJ, Hann AC, Furr JR, Russell AD. X-ray microanalysis of chlorhexidine-treated cells of *Saccharomyces cerevisiae*. *Lett Appl Microbiol* 1995;20:353–6.
- Hitchcock AP. aXis2000 is written in Interactive Data Language (IDL). It is available free for non-commercial use from <http://unicorn.mcmaster.ca/aXis2000.html>; 2006.
- Hope CK, Wilson M. Measuring the thickness of an outer layer of viable bacteria in an oral biofilm by viability mapping. *J Microbiol Methods* 2003;54:403–10.
- Hope CK, Wilson M. Analysis of the effects of chlorhexidine on oral biofilm vitality and structure based on viability profiling and an indicator of membrane integrity. *Antimicrob Agents Chemother* 2004;48:1461–8.
- Ikeda T, Tazuke S, Watanabe M. Interaction of biologically active molecules with phospholipid membranes. I. Fluorescence depolarization studies on the effect of polymeric biocide bearing biguanide groups in the main chain. *Biochim Biophys Acta* 1983;735:380–6.

- Jacobsen C, Wirick S, Flynn G, Zimba C. Soft X-ray spectroscopy from image sequences with sub-100 nm spatial resolution. *J Microsc* 2000;197:173–84.
- Kemner KM, Kelly SD, Lai B, Maser J, O'Loughlin EJ, Sholto-Douglas D, et al. Elemental and redox analysis of single bacterial cells by X-ray microbeam analysis. *Science* 2004;306:686–7.
- Khunkitti W, Hann AC, Lloyd D, Furr JR, Russell AD. X-ray microanalysis of chlorine and phosphorus content in biguanide-treated *Acanthamoeba castellanii*. *J Appl Microbiol* 1999; 86:453–9.
- Kilcoyne ALD, Steele WF, Fakra S, Hitchcock P, Franck K, Anderson E, et al. Interferometrically controlled scanning transmission microscopes at the Advanced Light Source. *J Synchrotron Radiat* 2003;10:125–36.
- Kolpin DW, Furlong ET, Meyer MT, Thurman EM, Zaugg SD, Barber LB, et al. Pharmaceuticals, hormones, and other organic wastewater contaminants in U.S. streams, 1999–2000: a national reconnaissance. *Environ Sci Technol* 2002;36:1202–11.
- Lawrence JR, Swerhone GDW, Neu TR. Design and evaluation of a simple rotating annular reactor for replicated biofilm studies. *J Microbiol Methods* 2000;42:215–24.
- Lawrence JR, Korber DR, Wolfaardt GM, Caldwell DE, Neu TR. Analytical imaging and microscopy techniques. In: Hurst CJ, Crawford RL, Knudsen GR, McInerney M, Stetzenbach LD, editors. *Manual of environmental microbiology*. 2nd ed. Washington, DC: American Society for Microbiology Press; 2002. p. 39–61.
- Lawrence JR, Swerhone GDW, Leppard GG, Araki T, Zhang X, West MM, et al. Scanning transmission X-ray, laser scanning, and transmission electron microscopy mapping of the exopolymeric matrix of microbial biofilms. *Appl Environ Microbiol* 2003;69:5543–54.
- Neu TR, Wöfl S, Lawrence JR. 3-dimensional differentiation of phototrophic biofilm constituents by multi channel confocal and 2-photon laser scanning microscopy. *J Microbiol Methods* 2004;56:161–72.
- Noll F, Sumper M, Hampp N. Nanostructure of diatom silica surfaces and of biomimetic analogues. *Nano Let* 2002;2:91–5.
- Pecher K, McCubbery D, Kneedler E, Rothe J, Bargar J, Meigs G, et al. Quantitative charge state analysis of manganese biominerals in aqueous suspension using scanning transmission X-ray microscopy (STXM). *Geochim Cosmochim Acta* 2003;67:1089–98.
- Ranganathan NS. Chlorhexidine. In: Ascenzi JM, editor. *Handbook of disinfection and antiseptics*. New York, NY: Marcel Dekker Inc.; 1996. p. 235–64.
- Russell AD. Similarities and differences in the response of microorganisms to biocides. *J Antimicrob Chemother* 2003; 52:750–63.
- Sette F, Sinkovic B, Ma YJ, Chen CT. Crystal-field splitting of core excitations in ionic crystals. *Phys Rev B* 1989;39:11125–30.
- Sicko-Goad L, Lazinsky D, Hall J, Simmons MS. Effects of chlorinated benzenes on diatom fatty acid composition and quantitative morphology. I. 1,2,4-Trichlorobenzene. *Arch Environ Contam Toxicol* 1989a;18:629–37.
- Sicko-Goad L, Hall J, Lazinsky D, Hall J, Simmons MS. Effects of chlorinated benzenes on diatom fatty acid composition and quantitative morphology. III. 1,2,3-Trichlorobenzene. *Arch Environ Contam Toxicol* 1989b;18:647–55.
- Suci PA, Geesey GG, Tyler BJ. Integration of Raman microscopy, differential interference contrast microscopy, and attenuated total reflection Fourier transform infrared spectroscopy to investigate chlorhexidine spatial and temporal distribution in *Candida albicans* biofilms. *J Microbiol Methods* 2001;46:193–208.
- Tanaka T, Murayama S, Tuda N, Nishiyama M, Nakagawa K, Matsuo Y, et al. Microbial degradation of disinfectants. A new chlorhexidine degradation intermediate (CHDI), CHDI-C, produced by *Pseudomonas* sp strain no. A-3. *J Health Sci* 2005; 51:357–61.
- Thomas B, Stickler DJ. Chlorhexidine resistance and the lipids of *Providencia stuartii*. *Microbios* 1979;24:141–50.
- Walters TH, Furr JR, Russell AD. Antifungal action of chlorhexidine. *Microbios* 1983;38:195–204.
- Warwick T, Ade H, Kilcoyne ALD, Kritscher M, Tyliczszak T, Fakra S, et al. A new bend magnet beam line for scanning transmission X-ray microscopy at the Advanced Light Source. *J Synchrotron Radiat* 2002;9:254–7.
- Wernert GT, Winkler DA, Holan G, Nicoletti G. Synthesis, biological activity, and QSAR studies of antimicrobial agents containing biguanide isosteres. *Aust J Chem* 2004;57:77–85.
- Wilson BA, Smith VH, Denoyelles Jr F, Larive CK. Effects of three pharmaceutical and personal care products on natural freshwater algal assemblages. *Environ Sci Technol* 2003;37:1713–9.
- Wolfaardt GM, Lawrence JR, Headley JV, Robarts RD, Caldwell DE. Microbial exopolymers provide a mechanism for bioaccumulation of contaminants. *Microb Ecol* 1994;27:279–91.